JACS
JOURNAL OF THE AMERICAN CHEMICAL SOCIETY
Communication
pubs.acs.org/JACS

o-Methoxy Substituents in Spiro-OMeTAD for Efficient Inorganic–Organic Hybrid Perovskite Solar Cells

Nam Joong Jeon,[†,§] Hag Geun Lee,[†,§] Young Chan Kim,[†] Jangwon Seo,[†] Jun Hong Noh,[†] Jaemin Lee,*[,†] and Sang Il Seok*[,†,‡]

[†]Division of Advanced Materials, Korea Research Institute of Chemical Technology, 141 Gajeong-Ro, Yuseong-Gu, Daejeon 305-600, Republic of Korea

[‡]Department of Energy Science, Sungkyunkwan University, Suwon 440-746, Republic of Korea

Supporting Information

ABSTRACT: Three spiro-OMeTAD derivatives have been synthesized and characterized by $^{1}H/^{13}C$ NMR spectroscopy and mass spectrometry. The optical and electronic properties of the derivatives were modified by changing the positions of the two methoxy substituents in each of the quadrants, as monitored by UV–vis spectroscopy and cyclic voltammetry measurements. The derivatives were employed as hole-transporting materials (HTMs), and their performances were compared for the fabrication of mesoporous $TiO_2/CH_3NH_3PbI_3$/HTM/Au solar cells. Surprisingly, the cell performance was dependent on the positions of the OMe substituents. The derivative with *o*-OMe substituents showed highly improved performance by exhibiting a short-circuit current density of 21.2 mA/cm^2, an open-circuit voltage of 1.02 V, and a fill factor of 77.6% under 1 sun illumination (100 mW/cm^2), which resulted in an overall power conversion efficiency (PCE) of 16.7%, compared to ∼15% for conventional *p*-OMe substituents. The PCE of 16.7% is the highest value reported to date for perovskite-based solar cells with spiro-OMeTAD.

Very recently, hybrid halide perovskites (e.g, methylammonium lead halides $CH_3NH_3PbX_3$, where X = halogen) were introduced as promising light harvesters in solar cells.[1−5] Mesoporous (mp) TiO_2 or Al_2O_3 was used as the scaffold for the perovskite absorbers in perovskite-based solar cells with hole-transporting materials (HTMs). In these cells, excited carriers can be injected into the hole- and electron-transporting materials for collection at the electrodes, and the perovskite itself can behave as an electron or hole transporter depending on the scaffold used.[1,3] Recently, planar heterojunctions with a bulk layer of perovskite acting as both the absorber and long-range transporter of charged species have shown the highest efficiencies.[6−8] Currently, most state-of-the-art perovskite-based devices utilize 2,2′,7,7′-tetrakis(*N*,*N*-bis(*p*-methoxyphenyl)amino)-9,9′-spirobifluorene (spiro-OMeTAD) as the HTM in their structures,[1,2,4−8] although other types of HTMs have been reported by several groups.[3,9,10] For example, Grätzel and co-workers reported a 15.0% power conversion efficiency (PCE) for nanoporous $TiO_2/CH_3NH_3PbI_3$/spiro-OMeTAD/Au.[5] Snaith et al.[6] showed a maximum PCE of 15.4% with an open-circuit voltage (V_{oc}) of 1.07 V and a short-circuit current density (J_{sc}) of 21.5 mA cm^{-2} using $CH_3NH_3PbI_{3-x}Cl_x$ deposited as thin layers with spiro-OMeTAD as the hole conductor. Initially, spiro-OMeTAD was used as a solid hole conductor in dye-sensitized solar cells (DSSCs), and it gave a PCE of 0.74% under full sunlight.[11] The PCE was increased to 2.56% under 1 sun illumination by the addition of 4-*tert*-butylpyridine (t-BP) and lithium bis(trifluoromethanesulfonyl)imide (LiTFSI) to spiro-OMeTAD.[12] This system was further optimized by increasing the hole mobility of spiro-OMeTAD by more than 1 order of magnitude through doping with a Co(III) complex and by using a high-absorption-coefficient organic dye, and a PCE of 7.2% was reported.[13]

Several attempts to develop alternative organic HTMs for sensitized solar cells have been made. Recently we successfully developed an efficient inorganic–organic hybrid solar cell using poly(3-hexylthiophene) (P3HT) and poly[*N*-9-heptadecanyl-2,7-carbazole-*alt*-3,6-bis(thiophen-5-yl)-2,5-dioctyl-2,5-dihydropyrrolo[3,4]pyrrole-1,4-dione] (PCBTDPP) as effective hole conductors and Sb_2S_3 or Sb_2Se_3 as sensitizers.[14−16] Also, P3HT, poly[2,6-(4,4-bis(2-ethylhexyl)-4*H*-cyclopenta[2,1-*b*;3,4-*b*′]dithiophene)-*alt*-4,7(2,1,3-benzothiadiazole] (PCPDTBT), and poly(triarylamine) (PTAA) were employed for the fabrication of hybrid halide perovskite solar cells.[3] However, most of the HTMs are made of polymers whose synthesis and purification are difficult, with the possible disadvantage of incomplete filling of the mp-TiO_2 with polymeric HTMs. Small molecular HTMs such as *N*,*N*′-dialkylperylenediimide (PDI) and *N*,*N*′-bis(3-methylphenyl)-*N*,*N*′-diphenylbenzidine (TPD) were also tried to increase the V_{oc} of perovskite solar cells.[10] Recently, we synthesized pyrenearylamine derivatives and applied them as HTMs in perovskite-based solar cells, but their performance was still poor compared with spiro-OMeTAD.[17]

From the perspective of the material's chemical structure, it is noteworthy that methoxy groups were introduced into spiro-OMeTAD in order to control the oxidation potential of the materials. The −OMe group is electron-withdrawing by the inductive effect, but it can also exhibit electron-donating behavior under resonance stabilization. Hammett has reported two opposite effects of the −OMe substituent depending on the substitution position in the aromatic ring: electron-donating at

Received: March 27, 2014
Published: May 16, 2014

   dx.doi.org/10.1021/ja502824c | J. Am. Chem. Soc. 2014, 136, 7837−7840

the para position and electron-withdrawing at the meta position.[18] In addition to such electronic effects, substitution at the ortho position can also influence the oxidation potential by steric effects. Therefore, a simple and effective strategy to fine-tune the electronic properties is to change the substitution position of the −OMe group in arylamine-based HTMs. There are no reports on the application of ortho and meta derivatives of spiro-OMeTAD as HTMs in perovskite-based solar cells. Hence, we decided to investigate the effect of replacing *p*-OMe groups in spiro-OMeTAD with *o*- and *m*-OMe groups [see Figure S1 in the Supporting Information (SI) for the molecular structures].

In this study, we systematically changed the position of −OMe substituents of spiro-type arylamine HTMs from para to meta and ortho and investigated their structure−property relationship in perovskite-based hybrid solar cells. Thus, we report the synthesis and characterization of three spiro-OMeTAD derivatives and their application in perovskite-based solar cells. The position of one of the two *p*-OMe substituents in each of the quadrants of spiro-OMeTAD was replaced with an *o*- or *m*-OMe substituent. The role of the −OMe group in the spiro-OMeTAD substituent is to adjust the electronic properties of the hole conductor. Surprisingly, the cell using the ortho-substituted derivative in spiro-OMeTAD showed better performance than the para- and meta-substituted derivatives, with an overall PCE of 16.7% under air-mass 1.5 global (AM 1.5G) illumination at 100 mW/cm^2; this is one of the highest PCEs reported to date for mp-TiO_2/$CH_3NH_3PbI_3$ perovskite/spiro-OMeTAD.

The procedure for the synthesis of the spiro-OMeTAD derivatives is shown in Figure 1, and experimental details are

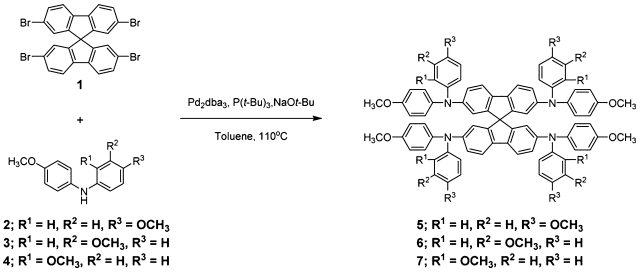

Figure 1. Synthetic route for spiro-OMeTAD derivatives.

provided in the SI. Spiro-OMeTAD derivatives were synthesized by the Buchwald−Hartwig amination reaction between 2,2′,7,7′-tetrabromo-9,9′-spirobifluorene (**1**) and the respective bis-(methoxyphenyl)amines containing *p*-OMe, *m*-OMe, or *o*-OMe substituents (**2**, **3**, and **4**, respectively). Compound **5**, which contains two *p*-OMe substituents in each of the quadrants, is the well-known compound spiro-OMeTAD, and in order to clearly define the substitution position, it is denoted as *pp*-spiro-OMeTAD in this study. The other two spiro-type arylamine derivatives with different substitution positions are denoted as *pm*-spiro-OMeTAD (**6**) and *po*-spiro-OMeTAD (**7**). All three spiro-OMeTAD compounds were purified by column chromatography followed by recrystallization and characterized by ^{1}H/^{13}C NMR spectroscopy and mass spectrometry (see the SI). All of the analytical data were consistent with the proposed structures. The three compounds have good solubility in all of the common organic solvents.

The UV−vis absorption spectra of the three spiro-OMeTAD derivatives in the film state are shown in Figure 2a. All of the derivatives showed absorption bands in the UV region, and the absorption maxima of *pp*-, *pm*-, and *po*-spiro-OMeTAD are

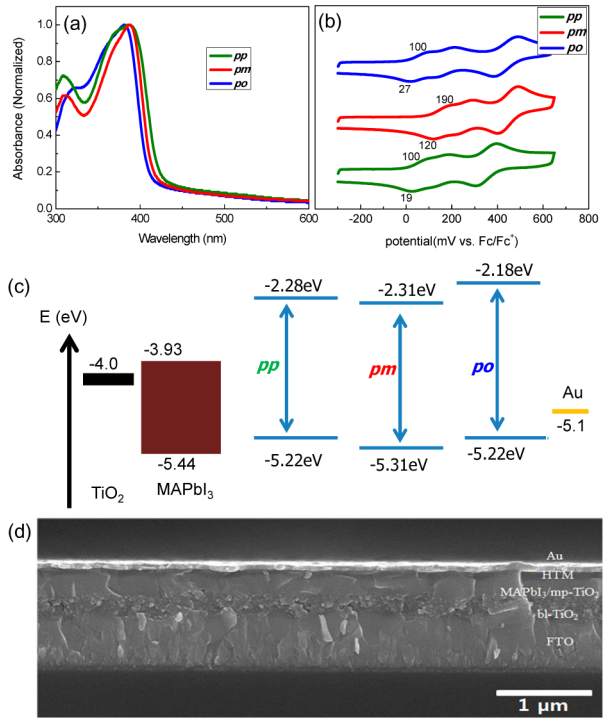

Figure 2. (a) UV−vis absorption spectra of *pp*-, *pm*-, and *po*-spiro-OMeTAD in chlorobenzene. (b) Cyclic voltammograms of *pp*-, *pm*-, and *po*-spiro-OMeTAD. (c) Energy level diagram for the corresponding materials used in our devices. (d) Cross-sectional structure of a representative device.

centered at 387, 387, and 381 nm, respectively. The absorption onset wavelength that reflects the optical band-gap energy of the material helps in identifying the influence of the substitution position. The absorption onsets of the three derivatives moved to shorter wavelength in going from *pp*- (423 nm) to *pm*- (413 nm) to *po*-spiro-OMeTAD (409 nm), which implies that the newly synthesized *pm*- and *po*-spiro-OMeTAD have increased band-gap energies relative to the well-known *pp*-spiro-OMeTAD.

In order to study the electrical properties of these compounds, we investigated the electrochemical properties by cyclic voltammetry (CV). As shown in Figure 2b, the three compounds showed similar cyclic voltammograms in the oxidation scan.[19] The first two overlapped oxidation peaks can be attributed to the two consecutive oxidation reactions of the molecule to generate a radical monocation and a quinoidal dication, respectively.[20] Interestingly, the change in the substitution position from para to meta resulted in an increased oxidation potential. This occurred because the *m*-OMe group exerts an electron-withdrawing effect while the *p*-OMe group exerts an electron-donating effect, as previously reported by Hammett.[18] However, contrary to meta substitution, substitution at the ortho position did not result in noticeable changes in the oxidation potential, which means that the electron-donating property of the −OMe group is maintained in ortho substitution. On the basis of the reported highest occupied molecular orbital (HOMO) energy of *pp*-spiro-OMeTAD (5.22 eV),[2] the HOMO energy levels of *pm*- and *po*-spiro-OMeTAD were calculated to be −5.31 and −5.22 eV, respectively.

Figure 2c shows an energy level diagram for the three spiro derivatives. The lowest unoccupied molecular orbital (LUMO) energies were calculated by adding the optical band-gap energies to the HOMO energies. The electronic effects of the spiro

dx.doi.org/10.1021/ja502824c | J. Am. Chem. Soc. 2014, 136, 7837−7840

derivatives were observed to change substantially depending on the substitution position. Compared with para substitution, meta substitution primarily decreased the HOMO energy (ca. 0.09 eV), mainly because of the electron-withdrawing effect of the *m*-OMe substituent, which does not contribute to resonance stabilization. On the other hand, ortho substitution increased the LUMO energy (ca. 0.10 eV), relative to the para case, mainly because of steric effects, that is, the band-gap energy increased conceivably because of the increased dihedral angle between the *o*-OMe-phenyl group and the fluorene ring, which decreases the effective conjugation of the molecule. The electron-donating effects of *o*- and *p*-OMe were almost the same, as revealed by the CV measurements.

We compared the similarities and differences in photovoltaic performance of the three spiro-OMeTAD derivatives as HTMs by fabricating perovskite-based solar cells. For cell fabrication, we used a solvent mixture of γ-butyrolactone and dimethyl sulfoxide to deposit a uniform $CH_3NH_3PbI_3$ ($MAPbI_3$) layer.[21] The cell was fabricated by spin-coating a layer of $MAPbI_3$ onto the mp-TiO_2 surface followed by drying at 100 °C. Spin coating of *pp*-, *pm*-, and *po*-spiro-OMeTAD as HTMs was accomplished with LiTFSI and t-BP dissolved in toluene. In this study, we did not incorporate hole dopants such as tris[2-(1*H*-pyrazol-1-yl)-4-*tert*-butylpyridine]cobalt(III) tris(bis(trifluoromethylsulfonyl)-imide) (FK209) because we could fabricate the cells with a very thin layer of spiro-OMeTAD. The same concentration was used for each spiro-OMeTAD derivative/toluene solution to maintain a very similar thickness of the HTM as an overlayer on the perovskite. Finally, the Au electrode was deposited on top by thermal evaporation to complete the solar cell structure. Figure 2d shows a cross-sectional image of the representative solar cell device fabricated in this work, as observed by scanning electron microscopy (SEM). As can be seen, the $MAPbI_3$ perovskite forms a thin (~350 nm) capping layer with full infiltration into the ~250 nm thick mp-TiO_2 layer and has a spiro-OMeTAD overlayer (~70 nm). The thicknesses of the *pp*-, *pm*-, and *po*-spiro-OMeTAD overlayers were similar, as estimated by the same molecular weight. The gold contact on top of this organic conductor can also be observed.

In Figure 2c, the band alignment of TiO_2, $MAPbI_3$, and the spiro-OMeTAD derivatives can be observed. The band alignment is such that exciton dissociation and charge transfer at the interface are energetically favorable with a possible driving force for hole transfer from $MAPbI_3$ into the spiro-OMeTAD derivative. Therefore, free charge carriers (or excitons) generated from the $MAPbI_3$ layer can be extracted (or dissociated) by transfer of an electron to the underlying mp-TiO_2 layer through hole transfer to the spiro-OMeTAD HTM. However, there was a large hysteresis and distortion in the current density−voltage (*J*−*V*) curves in the reverse (from V_{oc} to J_{sc}) and forward (from J_{sc} to V_{oc}) modes under standard AM 1.5G illumination for the perovskite-based solar cells, especially when they were measured at relatively short delay times.[21] Such hysteresis and discrepancy lead to over- or underevaluated performance, which induces a considerable error in measurement of the cell efficiency because reliable solar cell *J*−*V* measurements should exhibit coincident curves in the forward and reverse directions. Figure S2 shows the variation of the energy conversion efficiency for a representative solar cell (using *po*-spiro-OMeTAD as the HTM) measured by forward and reverse scans with 10 mV voltage steps and a delay time of 100 ms. Serious hysteresis between the two scan directions with different performance was observed; the efficiency in the reverse scan was 17.6%, while it was 14.1% in the forward scan. The efficiencies measured in the two scan directions decreased and increased symmetrically with increasing delay time and then matched at 1000 ms, but the average value remained almost the same after 300 ms (Figure S3). Therefore, in this work we show *J*−*V* curves obtained by averaging the *J*−*V* curves measured in the two scan directions with a delay time of 300 ms, because an excessively long measurement time is impractical.

With this in mind, we compared the photovoltaic performance of the cells fabricated using *pp*-, *pm*-, and *po*-spiro-OMeTAD. Figure 3a shows *J*−*V* curves for $TiO_2/MAPbI_3$/HTM/Au solar

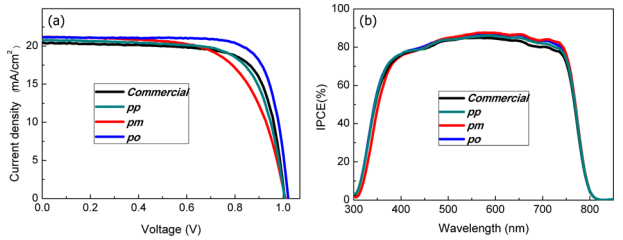

Figure 3. (a) *J*−*V* curves for $TiO_2/MAPbI_3$/HTM/Au devices fabricated with *pp*-, *pm*-, *po*- and commercial *pp*-spiro-OMeTAD as the HTM and (b) the corresponding IPCE spectra.

cells fabricated using the three HTMs, and the photovoltaic parameters of these devices are summarized in Table 1. In all

Table 1. Average Photovoltaic Parameters for Reverse- and Forward-Scanned $MAPbI_3$ Perovskite Solar Cells Using Commercial, *pm*-, *po*-, and *pp*-Spiro-OMeTAD as the HTM

HTM	J_{sc} (mA/cm²)	V_{oc} (V)	FF	PCE (%)	R_s (Ω)
commercial	20.4	1.00	73.7	15.2	37.35
pm	21.1	1.01	65.2	13.9	64.42
po	21.2	1.02	77.6	16.7	32.96
pp	20.7	1.00	71.1	14.9	45.37

three cases, an overlayer thickness of ~70 nm was observed in the SEM measurement (see Figure 2d). The device comprising mp-$TiO_2/MAPbI_3$/*pp*-spiro-OMeTAD gave V_{oc} = 1.00 V, J_{sc} = 20.7 mA cm^{-2}, a fill factor (FF) of 71.1%, and an overall PCE of 14.9%. These values and the cell performance are comparable to those of the cells fabricated with commercial *pp*-spiro-OMeTAD (Merck) as reported by Grätzel et al.[5] In contrast, the cells fabricated with *po*-spiro-OMeTAD exhibited dramatically enhanced performance compared with *pp*-spiro-OMeTAD cells, whereas the performance of cells fabricated from *pm*-spiro-OMeTAD was inferior. In Figure 3a, a small difference in J_{sc} and V_{oc} among the *pp*-, *pm*-, and *po*-spiro-OMeTAD derivatives with a large difference in FF is observed. Generally, in solar cells the series resistance (R_s) reduces the FF but does not affect V_{oc} and J_{sc} if it is not excessively high. A straightforward method of estimating R_s for a solar cell is to find the slope of the *J*−*V* curve near V_{oc}. As shown by the values in Table 1, *po*-spiro-OMeTAD-based cells showed the lowest R_s of 32.96 Ω, whereas the *pp*- and *pm*-spiro-OMeTAD cells showed R_s of 45.37 and 64.42 Ω, respectively. Besides R_s, the FF is also related to the shunt resistance (R_{sh}). In perovskite-based solar cells with an mp-TiO_2−perovskite composite/perovskite layer/HTM/Au structure, the HTM functions as both the hole-transporting layer and the electron-blocking layer.[3] *po*-Spiro-OMeTAD, with the highest LUMO, will block electron flow into the metal electrode,

dx.doi.org/10.1021/ja502824c | J. Am. Chem. Soc. 2014, 136, 7837−7840

which is responsible for increased R_{sh}. Therefore, *po*-spiro-OMeTAD effectively blocks the electrons and transports the holes from $MAPbI_3$ to the Au electrode. Accordingly, the superior performance of *po*-spiro-OMeTAD may be rationalized in terms of the increased FF value through a low R_s and a high R_{sh}. However, further studies are needed to quantify the extent of this effect among *pp*-, *pm*-, and *po*-spiro-OMeTAD. Figure 3b shows the monochromatic incident photon conversion efficiency (IPCE) spectra for the cells fabricated using *pp*-, *pm*-, *po*- and commercial *pp*-spiro-OMeTAD, and the integrated photocurrent densities are in good agreement with the values measured in the *J*−*V* curves, although the IPCE spectra differ slightly with wavelength.

In summary, we synthesized *pp*-, *pm*-, and *po*-spiro-OMeTAD derivatives that were applied as HTMs in $MAPbI_3$ pervoskite-based solar cells. On the basis of the CV measurements and UV−vis spectra, the HOMO and LUMO energies of each derivative were characterized. The derivatives were used to fabricate feasible perovskite-based solar cells. Energy conversion efficiencies of 16.7% were obtained, which is the highest value reported to date for perovskite-based solar cells with spiro-OMeTAD. The superior performance of *po*-spiro-OMeTAD is mainly attributed to the increased FF due to its low R_s and high R_{sh}. We believe that this study will open new avenues for the development of HTMs for perovskite-based solar cells for the fabrication of efficient and cost-effective photovoltaic devices.

■ ASSOCIATED CONTENT

Supporting Information

Experimental details and supporting figures. This material is available free of charge via the Internet at http://pubs.acs.org.

■ AUTHOR INFORMATION

Corresponding Authors

seoksi@krict.re.kr
jminlee@krict.re.kr

Author Contributions

[§]N.J.J. and H.G.L. contributed equally.

Notes

The authors declare no competing financial interest.

■ ACKNOWLEDGMENTS

This work was supported by the Global Research Laboratory (GRL) Program, the Global Frontier R&D Program on Center for Multiscale Energy System funded by the National Research Foundation in Korea, and by a grant from the KRICT 2020 Program for Future Technology of the Korea Research Institute of Chemical Technology (KRICT), Republic of Korea.

■ REFERENCES

(1) Lee, M. M.; Teuscher, J.; Miyasaka, T.; Murakami, T. N.; Snaith, H. J. *Science* **2012**, *338*, 643.
(2) Kim, H.-S.; Lee, C.-R.; Im, J.-H.; Lee, K.-B.; Moehl, T.; Marchioro, A.; Moon, S.-J.; Humphry-Baker, R.; Yum, J.-H.; Moser, J. E.; Grätzel, M.; Park, N.-G. *Sci. Rep.* **2012**, *2*, No. 591.
(3) Heo, J. H.; Im, S. H.; Noh, J. H.; Mandal, T. N.; Lim, C.-S.; Chang, J. A.; Lee, Y. H.; Kim, H.; Sarkar, A.; Nazeeruddin, M. K.; Grätzel, M.; Seok, S. I. *Nat. Photonics* **2013**, *7*, 486.
(4) Noh, J. H.; Im, S. H.; Heo, J. H.; Mandal, T. N.; Seok, S. I. *Nano Lett.* **2013**, *13*, 1764−1769.
(5) Burschka, J.; Pellet, N.; Moon, S.-J.; Humphry-Baker, R.; Gao, P.; Nazeeruddin, M. K.; Grätzel, M. *Nature* **2013**, *499*, 316.
(6) Liu, M.; Johnston, M. B.; Snaith, H. J. *Nature* **2013**, *501*, 395.
(7) Chen, Q.; Zhou, H.; Hong, Z.; Luo, S.; Duan, H.-S.; Wang, H.-H.; Liu, Y.; Li, G.; Yang, Y. *J. Am. Chem. Soc.* **2014**, *136*, 622.
(8) Liu, D.; Kelly, T. L. *Nat. Photonics* **2014**, *8*, 133.
(9) Giacomo, F. D.; Razza, S.; Matteocci, F.; D'Epifanio, A.; Licoccia, S.; Brown, T. M.; Carlo, A. D. *J. Power Sources* **2014**, *251*, 152.
(10) Edri, E.; Kirmayer, S.; Cahen, D.; Hodes, G. *J. Phys. Chem. Lett.* **2013**, *4*, 897.
(11) Bach, U.; Lupo, D.; Comte, P.; Moser, J. E.; Weissörtel, F.; Salbeck, J.; Spreitzer, H.; Grätzel, M. *Nature* **1998**, *395*, 583.
(12) Krüger, J.; Plass, R.; Cevey, L.; Piccirelli, M.; Grätzel, M.; Bach, U. *Appl. Phys. Lett.* **2001**, *79*, 2085.
(13) Burschka, J.; Dualeh, A.; Kessler, F.; Baranoff, E.; Cevey-Ha, N.-L.; Yi, C.; Nazeeruddin, M. K.; Grätzel, M. *J. Am. Chem. Soc.* **2011**, *133*, 18042.
(14) Chang, J. A.; Im, S. H.; Lee, Y. H.; Kim, H.-J.; Lim, C.-S.; Heo, J. H.; Seok, S. I. *Nano Lett.* **2012**, *12*, 1863.
(15) Choi, Y. C.; Mandal, T. N.; Yang, W. S.; Lee, Y. H.; Im, S. H.; Noh, J. H.; Seok, S. I. *Angew. Chem., Int. Ed.* **2014**, *53*, 1329.
(16) Choi, Y. C.; Lee, D. U.; Noh, J. H.; Kim, E. K.; Seok, S. I. *Adv. Funct. Mater.* **2014**, DOI: 10.1002/adfm.201304238.
(17) Jeon, N. J.; Lee, J.; Noh, J. H.; Nazeeruddin, M. K.; Grätzel, M.; Seok, S. I. *J. Am. Chem. Soc.* **2013**, *135*, 19087.
(18) Hammett, L. P. *J. Am. Chem. Soc.* **1937**, *59*, 96.
(19) Planells, M.; Abate, A.; Hollman, D. J.; Stranks, S. D.; Bharti, V.; Gaur, J.; Mohanty, D.; Chand, S.; Snaith, H. J.; Robertson, N. *J. Mater. Chem. A* **2013**, *1*, 6949.
(20) Seo, E. T.; Nelson, R. F.; Fritsch, J. M.; Marcoux, L. S.; Leedy, D. W.; Adams, R. N. *J. Am. Chem. Soc.* **1966**, *88*, 3498.
(21) Jeon, N. J.; Noh, J. H.; Kim, Y. C.; Yang, W. S.; Ryu, S.; Seok, S. I. Submitted.